IEEE Photonics Journal
An IEEE Photonics Society Publication

Open Access

An Optimized Attenuation Compensation and Contrast Enhancement Algorithm Without Pseudocharacteristics in Intravascular OCT Imaging

Volume 8, Number 5, October 2016

Yonghan Zhou
Tiegen Liu
Zhenyang Ding
Kuiyuan Tao
Kun Liu
Junfeng Jiang
Zixu Liu
Yongjun Jiang
Hao Kuang

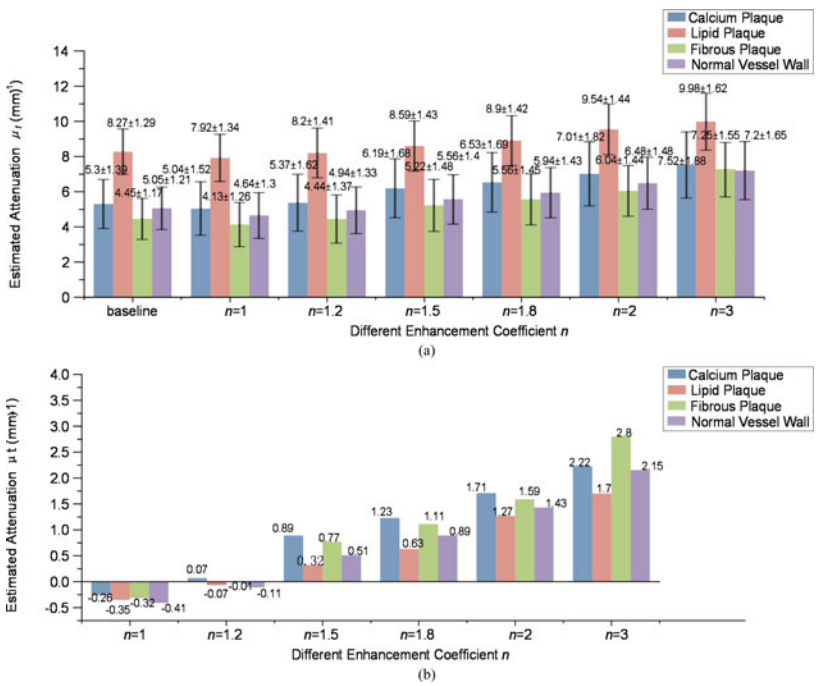

DOI: 10.1109/JPHOT.2016.2606239

An Optimized Attenuation Compensation and Contrast Enhancement Algorithm Without Pseudocharacteristics in Intravascular OCT Imaging

Yonghan Zhou,[1, 2] Tiegen Liu,[1, 2] Zhenyang Ding,[1, 2] Kuiyuan Tao,[1, 2, 3] Kun Liu,[1, 2] Junfeng Jiang,[1, 2] Zixu Liu,[3] Yongjun Jiang,[4] and Hao Kuang[3]

[1]College of Precision Instrument and Opto-Electronics Engineering, Tianjin University, Tianjin 300072, China
[2]Key Laboratory of Opto-Electronics Information Technical, Tianjin University, Ministry of Education, Tianjin 300072, China.
[3]Nanjing Forssmann Medical Technology Co., Nanjing 210002, China
[4]Department of Neurology, Jinling Hospital, Nanjing 210002, China

DOI:10.1109/JPHOT.2016.2606239

Manuscript received June 23, 2016; revised August 31, 2016; accepted September 1, 2016. Date of publication September 5, 2016; date of current version September 20, 2016. This work was supported in part by the National Natural Science Foundation of China under Grant 61505138, Grant 61475114, Grant 61108070, Grant 61227011, and Grant 61378043; in part by theTianjin Science and Technology Support Plan Program Funding under Grant 16JCQNJC01800; in part by the China Postdoctoral Science Foundation under Grant 2015M580199; in part by the National Basic Research Program of China (973 Program) under Grant 2010CB327806 and Grant 2010CB327802; in part by the National Instrumentation Program under Grant 2013YQ030915; in part by the Open Foundation of Key Laboratory of Opto-electronic Information Technology of Ministry of Education (Tianjin University) under Grant 2015KFKT023. Corresponding author: Z. Y. Ding (e-mail: zyding@tju.edu.cn).

Abstract: We present an optimized attenuation compensation and contrast enhancement algorithm to improve the quality of the intravascular optical coherence tomography (IVOCT) images and overcome the drawbacks of the previous algorithms, including pseudocharacteristics such as the variation of the tissue attenuation and the artifact shadows. We first analyze the variation of the tissue attenuation caused by the effect of the compensation and enhancement in theory. We compare the values of the estimated tissue attenuation in the baseline and enhanced IVOCT images with calcium, lipid, or fibrous plaques, respectively, to find an optimal enhancement coefficient preserving the attenuation characteristics. Then, we make a comparison of the IVOCT images with different values of the enhancement coefficient to evaluate the effects of each algorithm based on the improvement of visibility in depth, the contrast enhancement, and the preservation of characteristics. We point out that the optimizing attenuation coefficient for attenuation compensation and contrast enhancement algorithm could achieve the quality improvement of IVOCT images, as well as avoiding the pseudocharacteristics.

Index Terms: Coherence imaging, endoscopic imaging, optical coherence tomography

1. Introduction

Intravascular optical coherence tomography (IVOCT) [1] is a state-of-the-art technique for cardiovascular imaging. Based on a rotary catheter that emits near-infrared light with a fiber core,

IVOCT imaging system can produce high-resolution *in vivo* images of coronary artery structures for accurate real-time measurements. Tearney *et al.* first captured the *ex vivo* images of human coronary arteries by a catheter-based OCT system verifying its feasibility for assessing the atherosclerotic plaques microstructures [2]. Fujimoto *et al.* first demonstrated the ability of the catheter-based OCT system to perform ultrahigh resolution *in vivo* images of arterial tissues in animal studies [3]. Then, Tearney *et al.* reported the *in vivo* images of normal coronary arteries, intimal dissections, and deployed stents [4]. Jang *et al.* improved the outcome of the coronary intervention by first applying IVOCT to a human patient [5]. IVOCT system became commercially available when the M2 TD-OCT Imaging System (LightLab Imaging, Inc, becomes part of St. Jude Medical Inc, St. Paul, MN, USA) was released for sale in 2007 [6]. The FD-OCT system (C7-XRTM, LightLab Imaging, Inc.), which was approved by the Food and Drug Administration in the United States in 2010, was developed for a higher real-time imaging speed [7]. Dr. M. Costa performed the first U.S. IVOCT clinical case at the University Hospitals Case Medical Center in 2010 [8].

IVOCT system could assist interventional cardiologists in diagnosing by allowing the visibility of specific components of the atherosclerotic plaques and the implanted stents [9]. High-resolution IVOCT images enable the identification of the main plaque components including calcium, lipid, fibrous tissues, thrombus, and so on, and allow the evaluation of pathological situations before or after the implantation of stents [10], [11]. Therefore, the higher quality of coronary images and the quantitative analysis of plaque properties is significant for better interpretation of individual plaque components and more accurate assessment of the stents implantation.

The raw signal captured by IVOCT system is weak due to the rapid attenuation in tissues, and the back-scattered intensity decays with depth [12]. Therefore, the visibility enhancement in the deep tissue structures is an indispensable post-processing step for the higher quality of images and better interpretation of the coronary artery diseases. The algorithm of attenuation compensation and contrast enhancement in IVOCT imaging could significantly improve the quality of images including enhancing contrast, removing shadows from the dense structures, improving the visibility of deep tissues, revealing detail information of the atherosclerotic plaques and so on [13]–[15]. Hughes *et al*. presented a time-gain compensation algorithm for the sound signal attenuation in ultrasound imaging [16]. Girard *et al*. applied this compensation algorithm to OCT images of the human optic nerve head for the visibility of deep tissues and combine contrast enhancement to improve the quality of images [17]. Foin *et al*. implemented this algorithm to the IVOCT images allowing better visualization of coronary artery diseases [13]. However, we find that the previous algorithm [17] will cause pseudo characteristics such as the variation of the tissue attenuation and artifact shadows, which will mislead the doctors to make error diagnoses. As the tissue attenuation is a significant parameter to identify different plaque types such as calcium, lipid, fibrous plaques [18]–[20], its value variation will have a serious impact on the property identification of plaques. Additionally, when applying the previous algorithms [17] to IVOCT images with in-depth stents, we observe the artifact shadows in front of the stent struts in deep structures. Since the priority of medical image processing algorithms is to achieve better pathologic analysis, it is significant to optimize the algorithm for attenuation compensation and contrast enhancement, which can avoid generating the pseudo characteristics.

In this paper, we optimize the enhancement coefficient in the algorithm for the attenuation compensation and contrast enhancement to improve the quality of images without any pseudo characteristics in IVOCT imaging. Taking pseudo characteristics removal into consideration during the image processing in IVOCT, we first analyze the variation of the tissue attenuation caused by the effect of the compensation and enhancement in theory. We compare the values of the estimated tissue attenuation in baseline and enhanced IVOCT images with calcium, lipid, or fibrous plaques, respectively, to find the optimal enhancement coefficient which could preserve the attenuation characteristics that is an important feature for identifying the type of arterial plaques. Then we make a comparison of the IVOCT images applied the algorithms with different values of the enhancement coefficient, to choose a reasonable one for best effects. The evaluation results verify that the enhancement coefficient chosen to 1.2 in this paper could improve the quality of images without pseudo characteristics, by which will both have the effects of enhancing the visibility and contrast

in depth, diminishing the impact of shadow artifacts and maintaining the attenuation property of plaques.

2. Principle

To compensate the weak raw signal resulting from the rapid attenuation in tissues, the attenuation compensation and contrast enhancement algorithm [17] is given as

$$I_{en+comp}(z) = \frac{I^n(z)}{2\int_z^{\infty} I^n(u)du} \tag{1}$$

where $I_{en+comp}(z)$ is the enhanced and compensated intensity based on original intensity $I(z)$ at the depth z, and n is the exponent as an enhancement coefficient that determines the contrast or dynamic range of intensities. The proposed algorithm is applied to each pixel of the images to confirm that the resolution is not being degraded by it. Setting $1/2\int_z^{\infty} I(u)du$ as the compensation factor, the attenuation compensation effect is achieved by it. In addition, the contrast enhancement effect is achieved by the exponentiation n, where $n = 1$ means only compensation non enhancement, and greater n means higher contrast when $n > 1$.

To avoid over amplification of the noise in depth, an adaptive compensation method was developed and validated for ophthalmic OCT enhancement [21], which ought to improve the quality of IVOCT images. The core concept can be expressed as

$$I_{en+comp}(z) = \begin{cases} \frac{I^n(z)}{2\int_z^{\infty} I^n(u)du}, & E(z) \geq \text{t} \\ \frac{I^n(z)}{2t}, & E(z) < \text{t} \end{cases} \tag{2}$$

with

$$E(z) = \left[\int_z^{\infty} I^n(u)du\right]^2 \tag{3}$$

$$t = 0.1\%E_{\max}(z) = 0.1\% \times \max[E(z)] \tag{4}$$

where $E(z)$ is defined as the remaining energy that the accumulation of optical energy from the depth z to the end of this A-line, the lower value of which means the higher attenuation of tissues, and the compensation factor is relatively higher to increase the local intensity. Meanwhile, a threshold t is set to restrict the overcompensation in the deepest layer where the remaining energy is too low and only consists of the noise. When the remaining energy at a certain depth z_m falls below threshold, the compensation factor keeps constant to be $1/2t$ for z deeper than z_m.

Although this algorithm can enhance the contrast and compensate the attenuation, theoretically, it still has some issues to be solved. Firstly, the model of this algorithm [17] assumes the light is progressively attenuated by the local scattering due to the inhomogeneity and degradation of tissues, but the strong reflection such as the stent struts inside tissues are misleading factors for surrounding structures. The remaining energy for the local structure in front of stents has been largely increased because of the strong reflection of bare metal stents. Therefore, the value of the compensation factor is abnormally low, resulting in an inverse compensation which is counterproductive for structures in front of stents. When higher n leading a higher contrast, it will also obviously exacerbate this side-effect.

Second, this algorithm could cause a variation of the tissues attenuation μ_t, which is a significant parameter for the classification of different plaque types such as calcium, lipid, fibrous plaques [20]. In IVOCT system, the signal is modeled by an exponential decay curve. The detected response is given as

$$I(z) = I_0 T(z) S(z) \exp(-\mu_t z), \tag{5}$$

where I is the intensity, I_0 is the initial intensity, $T(z)$ is the confocal function with parameters of the catheter, and $S(z)$ is related to parameters of the light source, accounting for the swept source in

Fourier-domain OCT. By arranging and taking logarithm, we get a relationship of μ_t as

$$\ln\left[\frac{I(z)}{T(z)S(z)}\right] = \ln(I_0) - \mu_t z. \tag{6}$$

We use the equation $In(I_0) - \mu_t z$ to linearly fit the value set of $\ln[\frac{I(z)}{T(z)S(z)}]$; then, μ_t can be given as

$$\mu t = -\frac{d}{dz}\ln\left[\frac{I(z)}{T(z)S(z)}\right] = -\frac{dI(z)}{dz}\Big/ I(z) + \frac{dT(z)}{dz}\Big/ T(z) + \frac{dS(z)}{dz}\Big/ S(z). \tag{7}$$

In (7), the term of $-\frac{dI(z)}{dz}/I(z)$ is the dominant term for μ_t.

To analyze the variation of the tissue attenuation caused by the effects of the compensation and enhancement, we substitute $I_{en+comp}(z)$ in (1) to $I(z)$ in (7) and obtain the tissues attenuation by the effects of the compensation and enhancement $\mu_t^{en+comp}$ as

$$\mu_t^{en+comp} = -\frac{d}{dz}\ln\left[\frac{I_{en+comp}(z)}{T(z)S(z)}\right] = -n\frac{dI(z)}{dz}\Big/ I(z) - I^n(z)\Big/\int_z^\infty I^n(u)du + \frac{dT(z)}{dz}\Big/ T(z) + \frac{dS(z)}{dz}\Big/ S(z). \tag{8}$$

Comparing μt in (7) with $\mu_t^{en+comp}$ in (8), the term caused by the compensation effect $-I^n(z)/\int_z^\infty I^n(u)du$ is added in (8). As this term is opposite in sign with μ_t, the compensation effect will decrease the value of μ_t. The dominant term for μ_t is changed to $-n\frac{dI(z)}{dz}/I(z)$ caused by the enhancement effect, where $\frac{dI(z)}{dz}$ is a negative term. Therefore, that will increase the value of μ_t, and the higher value of n leads greater μ_t. As the compensation and enhancement effects on the variation of μ_t are opposite, we can choose a reasonable value of n to balance the influence on μ_t from the compensation and enhancement effects, which leads a minimal attenuation variation to preserve the attenuation characteristics.

3. Experimental Results and Discussion

3.1. Method

The optimal enhancement coefficient n can be evaluated in terms of the balance of the following factors: 1) the enhancement in deep tissues; 2) the contrast increment without artifacts; 3) the preservation of characteristics. Based on these principles, we compare the values of estimated μ_t in baseline and enhanced IVOCT images with calcium, lipid or fibrous plaques respectively, to find the optimal enhancement coefficient which leads a minimal attenuation variation. Then, we make a comparison of the IVOCT images applied the algorithms with different values of n to choose a reasonable one for best effects.

The clinic IVOCT images with atherosclerotic plaques in our experiments are selected for processing and analyzing from OCT images database of Jinling Hospital (Nanjing China). The raw data are exported from the IVOCT system (C7XR™, LightLab Imaging/St. Jude Medical, Westford, MA, USA) [22] for post-processing and frame analysis. The selections of frames include calcium, lipid and fibrous plaques, respectively, to verify the feasibility of the proposed algorithm for each plaque type. In addition, we apply this algorithm to the IVOCT images with stent struts in deep tissues.

3.2. Attenuation Estimation for Different Plaques With the Different Values of Enhancement Coefficient

We apply the fitting method described above in each A-line of the volume of interest (VOI) to attain a set of μt values then average them as a coefficient of each plaque type. Summary statistics consist of 150 VOIs which mostly include 20 to 50 A-lines and 20–50 sample pixels in each A-line, in 30 frames of IVOCT images with calcium, lipid, fibrous plaques, and normal vessel walls, respectively. Finally, we obtain the mean and standard deviation (SD) of the tissue attenuation μt for each type of

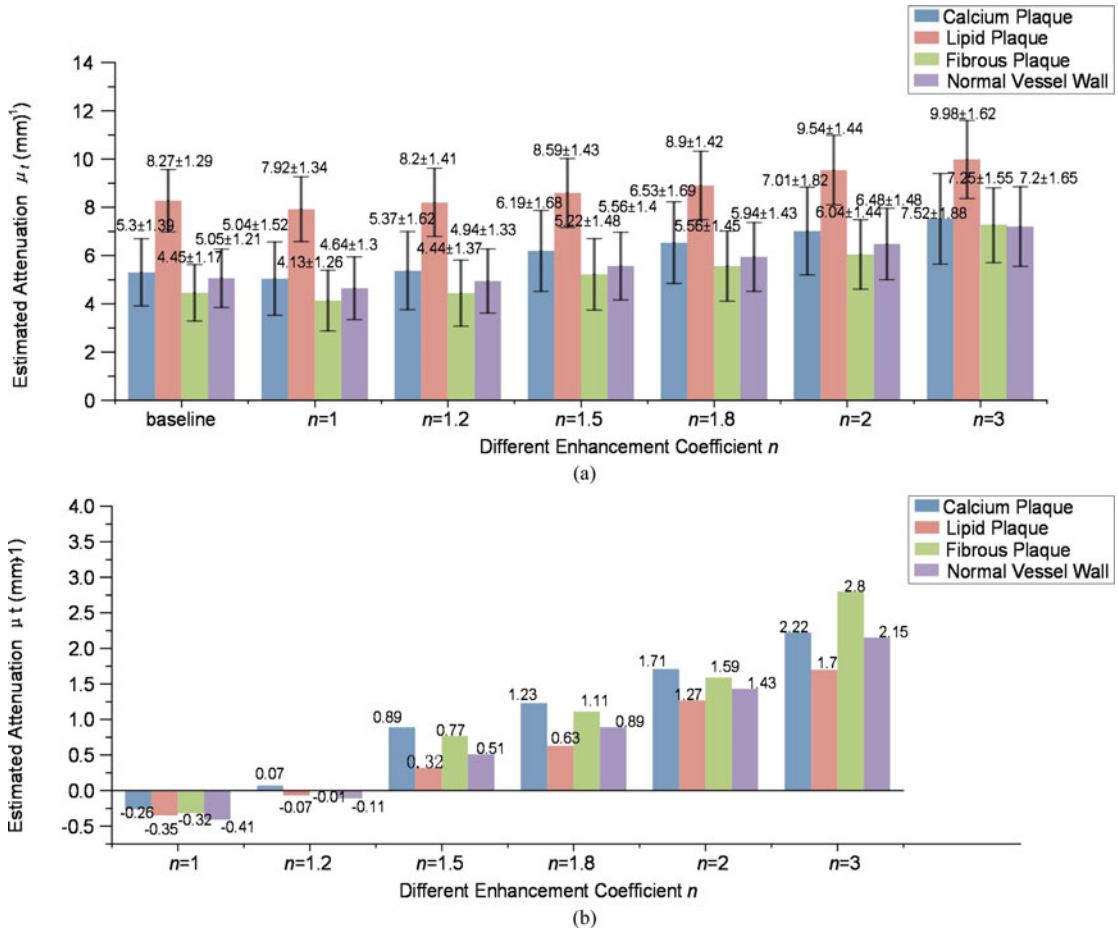

Fig. 1. (a) Comparison of the estimated attenuation μ_t of calcium, lipid, fibrous plaques, and normal vessel walls in baseline and enhanced IVOCT images with different values of the enhancement coefficient n, where values are mean±SD (mm^{-1}). (b) Comparison of the attenuation variation $\Delta\mu_t$ of calcium, lipid, fibrous plaques, and normal vessel walls in enhanced IVOCT images with different values of the enhancement coefficient n. For every type of tissue in the experiments, the value of the attenuation variation $\Delta\mu_t$ is negative when only compensated ($n = 1$), while it is positive and increased by the increment of the enhancement coefficient value when n>1. There is the minimal attenuation variation $\Delta\mu_t$ when the enhancement coefficient $n = 1.2$ in our experiments.

plaques in baseline images. Estimated values of the tissue attenuation μt conform with the values from previous studies[18–20] using the same IVOCT imaging system which are in the range from 2–7.1 mm^{-1} for calcium plaques, 7.62–18.2 mm^{-1} for lipid plaques, 1.07–7.6 mm^{-1} for fibrous plaques, and 2–5 mm^{-1} for normal vessel walls. The values of μt of different plaque types as calcium, lipid, fibrous plaques have a numerical difference, which is considered as a characteristic parameter for the classification of different plaque types. Additionally, the values of the normal vessel walls are estimated as a reference.

However, if the value of the attenuation largely changes caused by the processing algorithm, it will alter plaque characteristics and ultimately has a serious impact on the differentiation of calcium, lipid and fibrous plaques, which will obstruct doctors when identifying the different plaque types. Therefore, we estimate the values of the tissue attenuation μ_t of the same VOIs as above in enhanced and compensated images with different enhancement coefficient n and show in Fig. 1(a).

In addition, we define the attenuation variation $\Delta\mu_t$ as the change of estimated μ_t value from the baseline image to the compensated and enhanced images. We make a comparison of the attenuation variation when applying algorithm with different values of n to images with calcium, lipid, fibrous

plaques, and normal vessel walls, respectively, shown in Fig. 1(b). When focusing on the trends of $\Delta\mu_t$ with increment of n, we have observed that $\Delta\mu_t$ for fibrous plaques trends to rise while other tissue types trends to be relatively flat if further increasing the value of n. In this case, since fibrous plaques are characterized by the high intensity, low attenuation, and homogeneity [6], compared with other plaque types, the compensation factor $1/\int_z^\infty I^n(u)du$ of fibrous plaques (the second term in the (8) becomes relatively lower than others with the increment of n, which rises the value of μ_t and this relatively rising will appear when increasing n. In other word, the compensation effect of fibrous plaques becomes smaller than that of lipid and calcium plaques, which are both characterized by low intensity signal [6].

As the theory we mentioned above, the algorithm proposed by us consists of two effects, which are the attenuation compensation and the contrast enhancement. The compensation effect will decrease the value of the attenuation coefficient μ_t while the enhancement effect will increase it and the higher value of n leads greater attenuation. The statistics results shown in Fig. 1(b) have verified it. We mainly focus on the variation of the attenuation coefficient caused by the algorithm, which might cause doctors misidentify the plaque type by the altered value of attenuation coefficient into other plaque types according to the values in the baseline. Because we regard the attenuation coefficient measured in the baseline image as the standard data. Therefore, it is likely to incorrectly determine the plaque type by the estimated attenuation when a great variation of the attenuation coefficient appears. For example, in Fig. 1(a), the average value of attenuation coefficient for fibrous plaques has changed to 7.25 ± 1.55 when $n = 3$, which is close to the original value of attenuation coefficient for lipid plaques (8.27 ± 1.29) in the baseline image. Besides the numerical variation, it will also cause a corresponding characteristic variation. Especially for fibrous and lipid plaques, fibrous plaques are characterized by the high intensity, low attenuation, and homogeneity, while the characteristics of lipid plaques are a diffused border, low signal, high attenuation and inhomogeneity [6]. So there is a possibility to incorrectly determine fibrous plaques into lipid plaques, if the increased value of attenuation coefficient for the fibrous plaque falls into the value range of the lipid plaque. This is the reason we pointed out why doctors might make error diagnoses when differentiating plaque types.

To minimize the variation of attenuation coefficient, as the compensation and enhancement effects on the variation of the attenuation coefficient are opposite, we can choose a reasonable value of n to balance the influence on the attenuation coefficient from the compensation and enhancement effects. From the Fig. 1(b), when $n = 1.2$ in our experiments, we can obtain a minimal variation of μ_t, it can better preserve the attenuation characteristics and avoid misidentifying for the plaque type. As a reference, the estimated values of μ_t for the normal vessel walls verify the optimal choice of $n = 1.2$ can also hold for another tissue type in our experiments. Even though the attenuation coefficients of three different types of plaque and normal vessel walls are not absolutely invariable from those in baseline when $n = 1.2$, there is the relatively minimal variation for each tissue type at $n = 1.2$, which better preserves the attenuation characteristics in the medical Imaging. In general, the doctors identify the type of arterial plaques directly based on the characteristics of the medical Images such as morphology, attenuation and so on; therefore, it is very important to preserve any plaque characteristics after the imaging post-processing. Furthermore, to obtain more accurate attenuation parameter for the identification of plaque types, it is suggested to estimate the attenuation using the raw data of images because it varies with the application of the imaging post-processing.

3.3. IVOCT Images Analysis and Comparison With Different Enhancement Coefficient

Considering the influence on the attenuation characteristics from different values of n, we make a comparison of the IVOCT images with different values of n for the purpose of assessing the effects of each algorithm based on the improvement of visibility in depth, the contrast enhancement, and the preservation of characteristics.

Results here (see Fig. 2) indicate that the attenuation compensation and contrast enhancement algorithm could improve the quality of IVOCT images. It enhances the visibility of the deep tissue layers, reveal the detail information of the atherosclerotic plaques and improve the contrast of

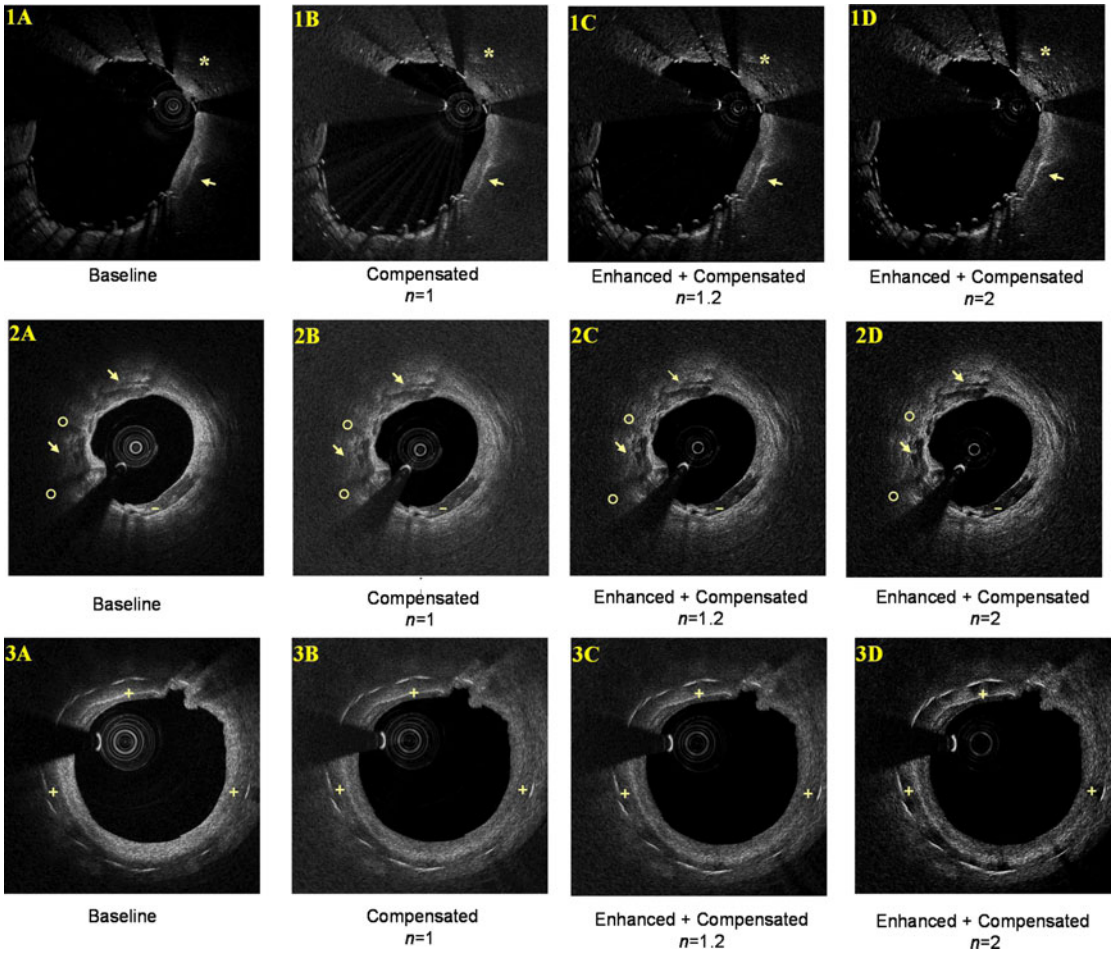

Fig. 2. In 1A-1D, the attenuation compensation and contrast enhancement algorithm improves the visibility and contrast of foam cells in depth (asterisk) comparing with the baseline images. In 2A-2D, the attenuation compensation and contrast enhancement algorithm improves the visibility and contrast of calcium plaque comparing with the baseline images. It also improves the identification of external contour and reveals detail information (arrow), and removes shadows caused by highly attenuating tissues (circle). To quantify the contrast enhancement, we calculate the boundary contrast that is defined as $C = |I_1 - I_2|/(I_1 + I_2)$,where I_1 and I_2 are the mean intensities of VOIs ($20 \times b$ pixels, where b is the number of pixels along the boundary) in front of and behind the boundary (arrow). Then, we obtain the boundary contrast $C_{1A} = 0.28$, $C_{1B} = 0.26$, $C_{1C} = 0.31$, $C_{1D} = 0.35$ in 1A-1D and $C_{2A} = 0.13$, $C_{2B} = 0.08$, $C_{2C} = 0.16$, $C_{2D} = 0.22$ in 2A-2D, respectively. In 3A-3D, applying to the IVOCT images with in-depth stents, the algorithm will produce obvious artifact shadows in front of stent struts comparing with the baseline images (cross). The higher n will bring about more obvious artifact shadows.

the plaque characteristics comparing with the baseline images. In detail, from the results of the boundary contrast, only compensating ($n = 1$) has decreased the contrast and dynamic range of intensities in a given image for the simultaneous observation of strong and week signal, while the image contrast has increased with the increment of $n (n > 1)$.

In the baseline images, limited by the rapid attenuation of the tissue, the contours of the atherosclerotic plaques and the detail information inside are not visible somewhat, shown in Fig. 2(1A, 2A). Compared with the baseline, the images only compensated could recover the weak signal and reveal the details of the plaque components in deep tissue structures. However, their contrast will decrease because of the increment of intensity in deep tissues, as shown in Fig. 2(1B, 2B). When $n > 1$, the algorithm for both compensation and enhancement can expand the dynamic range of intensities to enhance the contrast, making the plaques boundaries more visible and detectable.

However, we cannot unconditionally increase the value of n to enhance the contrast. Firstly, more speckle noise appears when further pursuing the increment of the boundary contrast [17]. Second, the value of attenuation coefficient changes greatly as we described above, leading a variation of attenuation characteristics that will confuse doctors for identification of plaque types. Additionally, by making a comparison of Fig. 2(1D, 2D, 3D) to Fig. 2(1C, 2C, 3C) respectively, we find that the higher value of n can make the contrast of the image enhances highly. But if the dynamic range has been largely expanded, the difference between strong and weak signal will be over-amplified even leading losses of information such as that shown in Fig. 2(2D) (hyphen). This phenomenon obviously appears when we apply the proposed algorithm to the IVOCT images with in-depth stents. Because more commonly, the images with complex components of the atherosclerotic plaques in deep structures also include the stents in depth. So we cannot avoid compensating the stents if an image both have the stents and plaques in depth. As we have shown in Fig. 2(3D), we find that further increasing n brings about pronounced shadow artifacts in front of stents, resulting in pseudo characteristics of IVOCT images. That is because the signal of stents does not conform with the law of the cardiovascular tissue attenuation. The strong reflection of bare metal stent struts makes the compensation factor of the structures in front of the stents largely decrease, misleading the local intensities relatively low and to form shadows. Then, the higher enhancement coefficient n that means stronger enhancement will lead the sharper contrast between the stents and the structures in front of those, exacerbating this side-effect.

Therefore, from this consideration, the value of enhancement coefficient n cannot be largely increased for preserving the attenuation characteristics and avoiding pronounced artifact shadows. As we discussed above, there is a relatively minimal attenuation variation when $n = 1.2$. It could better preserve the attenuation characteristics of plaque tissues as well as allow a combination of the moderate adjustment for the contrast and compensation for information in deep tissues. A reasonable n ($n = 1.2$ in our experiments) in this algorithm could result in preservation of attenuation coefficient, improving the quality of images without any pseudo characteristics.

4. Conclusion

We optimize the enhancement coefficient in the attenuation compensation and contrast enhancement algorithm to both achieve the quality improvement of IVOCT images and the removal of pseudo characteristics. Not only will the contrast and visibility of the deep tissue increase and more detail information of the atherosclerotic plaques be revealed by the optimized compensation and enhancement algorithm, but it will also avoid shadow artifacts and better preserve attenuation characteristics of IVOCT images.

Appendix A
Detail Derivation of $\mu_t^{en+comp}$ Estimation

We substitute $I_{en+comp}(z)$ in (1) to $I(z)$ in (7), $\mu_t^{en+comp}$ can be expressed as

$$\begin{aligned}
\mu_t^{en+comp} &= -\frac{d}{dz}\ln\left[\frac{I_{en+comp}(z)}{T(z)S(z)}\right] = -\frac{dI_{en+comp}(z)}{dz}\Big/ I_{en+comp}(z) + \frac{dT(z)}{dz}\Big/ T(z) + \frac{dS(z)}{dz}\Big/ S(z) \\
&= -\frac{d\left[\frac{I^n(z)}{2\int_z^\infty I^n(u)du}\right]}{dz}\Big/ \frac{I^n(z)}{2\int_z^\infty I^n(u)du} + \frac{dT(z)}{dz}\Big/ T(z) + \frac{dS(z)}{dz}\Big/ S(z) \\
&= -\frac{2\int_z^\infty I^n(u)du}{I^n(z)}\cdot\frac{nI^{n-1}(z)\frac{dI(z)}{dz}\cdot 2\int_z^\infty I^n(u)du - I^n(z)\cdot(-2I^n(z))}{\left[2\int_z^\infty I^n(u)du\right]^2} + \frac{dT(z)}{dz}\Big/ T(z) + \frac{dS(z)}{dz}\Big/ S(z) \\
&= -n\frac{dI(z)}{dz}\Big/ I(z) - I^n(z)\Big/\int_z^\infty I^n(u)du + \frac{dT(z)}{dz}\Big/ T(z) + \frac{dS(z)}{dz}\Big/ S(z). \qquad \text{(A1)}
\end{aligned}$$

References

[1] P. Patwari *et al.*, "Assessment of coronary plaque with optical coherence tomography and high-frequency ultrasound," *Amer. J. Cardiol.*, vol. 85, no. 5, pp. 641–644, 2000.

[2] G. J. Tearney *et al.*, "Catheter-based optical imaging of a human coronary artery," *Circulation*, vol. 94, no. 11, pp. 3013–3013, 1996.

[3] J. Fujimoto, S. A. Boppart, G. Tearney, B. Bouma, C. Pitris, and M. Brezinski, "High resolution in vivo intra-arterial imaging with optical coherence tomography," *Heart*, vol. 82, no. 2, pp. 128–133, 1999.

[4] G. J. Tearney *et al.*, "Porcine coronary imaging in vivo by optical coherence tomography," *Acta Cardiologica*, vol. 55, no. 4, pp. 233–237, 2000.

[5] I.-K. Jang, G. Tearney, and B. Bouma, "Visualization of tissue prolapse between coronary stent struts by optical coherence tomography comparison with intravascular ultrasound," *Circulation*, vol. 104, no. 22, pp. 2754–2754, 2001.

[6] H. G. Bezerra, M. A. Costa, G. Guagliumi, A. M. Rollins, and D. I. Simon, "Intracoronary optical coherence tomography: A comprehensive review: Clinical and research applications," *JACC: Cardiovascular Interventions*, vol. 2, no. 11, pp. 1035–1046, 2009.

[7] J. M. Schmitt, D. Adler, and C. Xu, "Intravascular OCT," *Opt. Coherence Tomography: Technol. Appl.*, vol. 71, pp. 2153–2172, 2015.

[8] Z. Wang, "Intravascular optical coherence tomography image analysis," P.hD. dissertation, Dept. Biomed. Eng., Case Western Reserve Univ., Cleveland, OH, USA, 2013.

[9] J. Ligthart, N. Bruining, and G. van Soest, "The diagnostic value of intracoronary optical coherence tomography," *Herz*, vol. 36, no. 5, pp. 417–429, 2011.

[10] O. Meissner *et al.*, "Intravascular optical coherence tomography: Differentiation of atherosclerotic plaques and quantification of vessel dimensions in crural arterial specimens," *RoFo: Fortschritte auf dem Gebiete der Rontgenstrahlen und der Nuklearmedizin*, vol. 178, no. 2, pp. 214–220, 2006.

[11] N. Gonzalo *et al.*, "Optical coherence tomography assessment of the acute effects of stent implantation on the vessel wall: A systematic quantitative approach," *Heart*, vol. 95, no. 23, pp. 1913–1919, 2009.

[12] F. Prati *et al.*, "Expert review document on methodology, terminology, and clinical applications of optical coherence tomography: Physical principles, methodology of image acquisition, and clinical application for assessment of coronary arteries and atherosclerosis," *Eur. Heart J.*, vol. 31, no. 4, pp. 401–415, 2010.

[13] N. Foin, J. M. Mari, J. E. Davies, C. Di Mario, and M. J. Girard, "Imaging of coronary artery plaques using contrast-enhanced optical coherence tomography," *Eur. Heart J.-Cardiovascular Imaging*, vol. 14, no. 1, pp. 85–85, 2013.

[14] N. Foin, *et al.*, "Intracoronary imaging using attenuation-compensated optical coherence tomography allows better visualisation of coronary artery diseases," *Cardiovascular Revascularization Med.*, vol. 14, no. 3, pp. 139–143, 2013.

[15] R. Lee *et al.*, "Intravascular assessment of arterial disease using compensated OCT in comparison with histology," *JACC: Cardiovascular Imaging*, vol. 9, no. 3, pp. 321–322, 2015.

[16] D. I. Hughes and F. A. Duck, "Automatic attenuation compensation for ultrasonic imaging," *Ultrasound Med. Biol.*, vol. 23, no. 5, pp. 651–664, 1997.

[17] M. J. Girard, N. G. Strouthidis, C. R. Ethier, and J. M. Mari, "Shadow removal and contrast enhancement in optical coherence tomography images of the human optic nerve head," *Investigative Ophthalmo. Vis. Sci.*, vol. 52, no. 10, pp. 7738–7748, 2011.

[18] C. Xu, J. M. Schmitt, S. G. Carlier, and R. Virmani, "Characterization of atherosclerosis plaques by measuring both backscattering and attenuation coefficients in optical coherence tomography," *J. Biomed. Opt.*, vol. 13, no. 3, 2008, Art. no. 034003.

[19] G. Van Soest *et al.*, "Atherosclerotic tissue characterization in vivo by optical coherence tomography attenuation imaging," *J. Biomed. Opt.*, vol. 15, no. 1, 2010, Art. no. 011105.

[20] M. Gargesha *et al.*, "Parameter estimation of atherosclerotic tissue optical properties from three-dimensional intravascular optical coherence tomography," *J. Med. Imaging*, vol. 2, no. 1, 2015, Art. no. 016001.

[21] J. M. Mari, N. G. Strouthidis, S. C. Park, and M. J. Girard, "Enhancement of lamina cribrosa visibility in optical coherence tomography images using adaptive compensation improving lamina cribrosa visibility in OCT images," *Investigative Ophthalmo. Vis. Sci.*, vol. 54, no. 3, pp. 2238–2247, 2013.

[22] S.J.Medical. "C7-XR^{TM} OCT Intravascular Imaging System," 2015. [Online]. Available: http://professional-intl.sjm.com/products/vas/intravascular-diagnostics-imaging/ffr-oct/c7-xr-oct-intravascular-imaging-system.